Environmental Science & Technology

Article

pubs.acs.org/est

# Speciation of Zn in Blast Furnace Sludge from Former Sedimentation Ponds Using Synchrotron X-ray Diffraction, Fluorescence, and Absorption Spectroscopy

Ruben Kretzschmar,*[,†] Tim Mansfeldt,[‡] Petar N. Mandaliev,[†] Kurt Barmettler,[†] Matthew A. Marcus,[§] and Andreas Voegelin[†,∥]

[†]Institute of Biogeochemistry and Pollutant Dynamics, ETH Zurich, CHN, 8092 Zurich, Switzerland

[‡]Soil Geography/Soil Science, Department of Geosciences, University of Cologne, Albertus-Magnus-Platz, D-50923 Köln, Germany

[§]Advanced Light Source, Lawrence Berkeley National Laboratory, 1 Cyclotron Road, Berkeley, California 94720, United States

[∥]Eawag, Swiss Federal Institute of Aquatic Science and Technology, Überlandstrasse 133, CH-8600 Dübendorf, Switzerland

Supporting Information

**ABSTRACT:** Blast furnace sludge (BFS), an industrial waste generated in pig iron production, typically contains high contents of iron and various trace metals of environmental concern, including Zn, Pb, and Cd. The chemical speciation of these metals in BFS is largely unknown. Here, we used a combination of synchrotron X-ray diffraction, micro-X-ray fluorescence, and X-ray absorption spectroscopy at the Zn K-edge for solid-phase Zn speciation in 12 BFS samples collected on a former BFS sedimentation pond site. Additionally, one fresh BFS was analyzed for comparison. We identified five major types of Zn species in the BFS, which occurred in variable amounts: (1) Zn in the octahedral sheets of phyllosilicates, (2) Zn sulfide minerals (ZnS, sphalerite, or wurtzite), (3) Zn in a KZn−ferrocyanide phase ($K_2Zn_3[Fe(CN)_6]_2 \cdot 9H_2O$), (4) hydrozincite ($Zn_5(OH)_6(CO_3)_2$), and (5) tetrahedrally coordinated adsorbed Zn. The minerals franklinite ($ZnFe_2O_4$) and smithsonite ($ZnCO_3$) were not detected, and zincite (ZnO) was detected only in traces. The contents of ZnS were positively correlated with the total S contents of the BFS. Similarly, the abundance of the KZn−ferrocyanide phase was closely correlated with the total CN contents, with the stoichiometry suggesting this as the main cyanide phase. This study provides the first quantitative Zn speciation in BFS deposits, which is of great relevance for environmental risk assessment, the development of new methods for recovering Zn and Fe from BFS, and potential applications of BFS as sorbent materials in wastewater treatment.

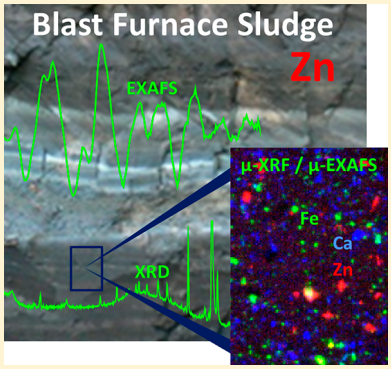


## INTRODUCTION

Blast furnace sludge (BFS) is a hazardous industrial waste generated in large quantities during the purification of flue gas leaving blast furnaces used in pig iron production.[1,2] During the past decades, the steel industry in Europe alone generated up to 500 000 t (dry mass) of BFS each year.[1] Typically, BFS contains large amounts of Fe (210−320 g $kg^{-1}$) and C (150−350 g $kg^{-1}$), besides major amounts of Si, Al, Ca, Mg, K, S, and potentially toxic trace metals such as Zn, Pb, and Cd.[1,3] The mineralogical composition of BFS typically includes calcite ($CaCO_3$), hematite ($\alpha$-$Fe_2O_3$), magnetite ($Fe_3O_4$), wüstite (FeO), and quartz ($SiO_2$). In addition, smaller amounts of graphite, $\alpha$-iron, dolomite ($CaMgCO_3$), siderite ($FeCO_3$), maghemite ($\gamma$-$Fe_2O_3$), iron cyanides, clay minerals, and layered-double-hydroxide (LDH) type minerals have been detected.[1−4] However, a very large fraction of BFS is usually X-ray amorphous material, which consists mainly of coke but may also include yet unidentified, amorphous or short-range ordered mineral phases.[2]

The high contents of Zn (10−32 g $kg^{-1}$) are currently the major obstacle preventing the recycling of BFS to the blast furnace for recovering the Fe as pig iron, because Zn would evaporate and condense on furnace walls causing considerable damage.[1,3] For this reason, vast quantities of BFS have been deposited in sedimentation ponds, which is today causing considerable environmental concerns due to the high contents of cyanides (0.3−5.5 g $kg^{-1}$), Pb (3−12 g $kg^{-1}$), Cd (31−227 mg $kg^{-1}$), Cr (26−238 mg $kg^{-1}$), As (25−276 mg $kg^{-1}$), and other toxic trace elements.[1,2,4] Recently, there is growing interest in new approaches for removing Zn and Pb from BFS, for example, by hydrometallurgical processes such as leaching under both acidic and oxidizing conditions.[1,3]

The chemical speciation of Zn, Pb, and other trace metals in BFS is still largely unknown, despite the fact that the

Received: July 23, 2012
Revised: September 29, 2012
Accepted: October 5, 2012

 © XXXX American Chemical Society 

bioavailability, toxicity, and leachability of these metals depend on their speciation. Van Herck et al.[1] found that a high removal efficiency of Zn from BFS by chemical extraction was achieved at pH values below 1.5 and redox potentials above +0.65 V. The largest fractions were extracted under acidic conditions, but 16−18% of the total Zn could only be extracted in an oxidizing acid medium. The residual Zn phases identified by X-ray diffraction (XRD) included sphalerite ($\beta$-ZnS) and franklinite ($ZnFe_2O_4$), but these Zn species accounted only for a minor fraction of the total Zn. From the abundance of Zn and cyanides in BFS, Steuer[5] postulated the possible occurrence of slightly soluble $Zn(CN)_2$, but no further analyses were performed at the time. In contrast, later studies failed to identify any crystalline Zn or Pb species in BFS from Germany using XRD analysis, with the exception of minor amounts of potassium zinc hexacyanoferrate(II)−nonahydrate, $K_2Zn_3[Fe(CN)_6]_2 \cdot 9H_2O$, that was detected by powder XRD.[2,6] If one assumes that all the cyanide in BFS occurs as $K_2Zn_3[Fe(CN)_6]_2 \cdot 9H_2O$, it is possible to calculate the proportion of Zn that may be bound in this compound.[2] On average, only 3% of Zn could be bound in this cyanide-containing phase. Other authors proposed that Zn may be present as sphalerite, franklinite, smithsonite ($ZnCO_3$), or zincite (ZnO) but without analytical proof. Thus, the question remains which other Zn species are present in BFS. The majority of Zn appears to be present in amorphous or short-range ordered solid phases that cannot be identified by conventional XRD analysis.

The objectives of the present study were (i) to identify and quantify the major and minor Zn species in BFS deposits at former sedimentation ponds using a combination of synchrotron XRD, X-ray fluorescence (XRF), and X-ray absorption spectroscopy (XAS) and (ii) to relate the Zn speciation to the chemical composition of the BFS, in particular, sulfur and cyanide (CN) contents.

## ■ MATERIALS AND METHODS

**Field Site and Sampling.** Samples were collected in 1998 and 2000 at a former BFS deposit located near Herne-Wanne in the Ruhr area, North-Rhine Westphalia, Germany.[2] The deposit consisted of nine open sedimentation ponds covering an area of ∼4 ha (Figure S1, Supporting Information), which were delivered with BFS from ∼1930 to 1982, resulting in sediment depths of up to 10 m and a sediment volume of ∼250 000 $m^3$.[2] At the time of sampling, the sludge sediments were uncovered and vegetated by birch trees. In 1998, 10 sampling pits were excavated to 110−150 cm depth on 6 of the former sedimentation ponds (ponds A−F), and BFS samples were collected from various depths below the soil surface. The sludge samples were dried at 50 °C and homogenized, and subsamples were finely ground in an agate ball mill (PM 4000, Retsch, Germany). Additionally, an undisturbed BFS sample was collected from a pit in pond A (∼60 cm depth; Figure S2, Supporting Information), air-dried, and subsequently embedded under vacuum in trace metal free, ultralow viscosity resin (LR White, polyhydroxy-aromatic acrylic resin; SPI Supplies, West Chester, PA). After curing at 60 °C for 48 h, 30 $\mu$m thin sections were prepared and mounted on pure $SiO_2$ slides for $\mu$-XRF and $\mu$-XAS analyses (Labor Beckmann, Schwülper-Lagesbüttel, Germany). In 2000, additional samples were collected at greater depth (up to 22 m) using a sediment coring device (18 cm core diameter). The samples were prepared for chemical and mineralogical analyses as described above. Additionally, one fresh BFS (sample BFS-2153) obtained from the active blast furnace Schwelgern 2 in Duisburg, Germany, was analyzed for comparison. Analyses of selected samples measured in 2003 and 2010 indicated no changes in Zn speciation during storage of dried BFS samples.

**Chemical Analyses.** All samples were analyzed for pH, total elemental composition, contents of total carbon ($C_{tot}$) and carbonate carbon ($C_{carb}$) carbon, and total cyanide (CN). The pH values were measured after equilibrating 10 g of BFS with 25 mL of doubly deionized (DDI) water (18.2 MΩ cm; Milli-Q, Millipore, USA). Elemental composition ($z \geq 11$ elements) was determined by wavelength-dispersive X-ray fluorescence analysis (Philips PW1400 and PW2404) on fused (1200 °C, 20 min) LiBr pellets containing 1 g of sample plus 5 g of $LiBO_2 \cdot 2H_2O$ and 25 mg of LiBr. A Cr tube (Cr K$\alpha$, 5415 eV) was used for the analysis of Ti, Ca, K, Cl, Ba, Cs, Sb, and Sn and a Rh tube (Rh K$\alpha$, 20216 eV) for the analysis of all other elements.

Total carbon, nitrogen, and sulfur contents were measured on a CHNS analyzer (Vario EL, Elementar, Germany). Carbonate carbon contents were determined by adding $HClO_4$ (15%) to 250 mg of samples that were preheated to 60 °C (TR 3600, Deltronik, Germany). The evolved $CO_2$ was absorbed in an alkaline solution and detected by Coulomb electrochemical titration. Noncarbonate carbon contents were calculated by the difference ($C_{noncarb} = C_{tot} - C_{carb}$).

Total contents of cyanide (CN) were determined by UV−vis absorption on a double-beam spectrophotometer (Lambda 2, Perkin−Elmer, Germany) at 600 nm after extraction of BFS (250−1000 mg) with 100 mL of 1 M NaOH using an acid microdistillation technique (MicroDistiller, Eppendorf, Germany) and addition of chloramine-T and pyridine−barbituric acid reagent.[7]

**X-ray Diffraction and Rietveld Analysis.** For mineralogical characterization and quantification of major mineral phases, all samples were analyzed by powder X-ray diffraction (Siemens D-500, Siemens, Germany) using Cu K$\alpha$ radiation (8041 eV; $\lambda$ = 1.5418) from 2 to 72° 2$\theta$ using a step size of 0.01° 2$\theta$ and a dwell-time of 10 s per step. Selected XRD patterns were analyzed by Rietveld refinement using AutoQuan software.[2]

Since, with the exception of $K_2Zn_3[Fe(CN)_6]_2 \cdot 9H_2O$, no crystalline Zn phases could be detected by conventional XRD, we carried out additional synchrotron XRD measurements at the powder diffraction station of the Materials Sciences (MS-Powder) beamline at the Swiss Light Source (SLS). Synchrotron XRD measurements were performed in Debye−Scherrer (transmission) geometry using cylindrical borosilicate 0.3 mm diameter capillaries spun for improved powder averaging. Powder patterns were collected up to 2$\theta$ = 120° with a MYTHEN-II silicon strip detector at an incident X-ray energy of 27 973 eV ($\lambda$ = 0.4432 Å), calibrated using $LaB_6$ (NIST 660b line position standard) contained in a 0.3 mm capillary.

**Microfocused X-ray Fluorescence and X-ray Absorption Spectroscopy.** Based on preliminary examination of the thin sections on an optical microscope and a benchtop $\mu$-XRF instrument, we selected typical regions for more detailed analyses by synchrotron $\mu$-XRF and $\mu$-XAS analyses at Beamline 10.3.2 of the Advanced Light Source (ALS, Berkeley, CA).[8] Elemental distribution maps for Zn, Fe, Ca, and other elements were collected using step sizes between 3 and 10 $\mu$m with beam spot sizes between 3 × 3 and 15 × 6 $\mu m^2$, depending on the size of the mapped region. The incoming X-ray energy

**Table 1. Color, pH, Elemental Composition, Cyanide Content, and Mineralogy of Selected BFS Samples from a Former Sedimentation Pond Site in Herne-Wanne, Germany[a]**

| parameter | unit | sample | | | | |
|---|---|---|---|---|---|---|
| | | D-2125 | E-2128 | B-2113 | C-2123 | BFS-2153[b] |
| depth | cm | 60−120 | 80−120 | 10−23 | 85−120 | — |
| color[c] | — | black | dark gray | gray | black | black |
| pH ($H_2O$) | — | 7.1 | 8.4 | 8.2 | 7.8 | 7.9 |
| $C_{carb}$[d] | g $kg^{-1}$ | 8.2 | 20.7 | 17.8 | 15.5 | nd |
| $C_{noncarb}$[d] | g $kg^{-1}$ | 143 | 104 | 77 | 282 | nd |
| Fe | g $kg^{-1}$ | 132.6 | 185.5 | 113.7 | 79.3 | 205.3 |
| Al | g $kg^{-1}$ | 27.8 | 37.5 | 44 | 33.6 | 9.3 |
| Si | g $kg^{-1}$ | 135.6 | 81.8 | 100.4 | 69.5 | 21.8 |
| Ca | g $kg^{-1}$ | 36.7 | 83.2 | 105.6 | 63.6 | 22.4 |
| Mg | g $kg^{-1}$ | 9 | 19.7 | 16.9 | 10.4 | 2.6 |
| K | g $kg^{-1}$ | 3.98 | 9.88 | 14.19 | 7.55 | 13 |
| S | g $kg^{-1}$ | 4.55 | 3.13 | 3.94 | 15.84 | 13.54 |
| CN | mg $kg^{-1}$ | 1868 | 3231 | 4075 | 1427 | 6034 |
| Zn | mg $kg^{-1}$ | 25 802 | 23 869 | 17 566 | 44 430 | 21 870 |
| Pb | mg $kg^{-1}$ | 9574 | 4763 | 8525 | 1420 | 3637 |
| Cd | mg $kg^{-1}$ | 18.7 | 42.6 | 22.7 | 30.0 | nd |
| As | mg $kg^{-1}$ | 109 | 94 | 124 | 25 | 76 |
| amorphous | g $kg^{-1}$ | 723.2 | 694.5 | 488.9 | 501.9 | nd |
| calcite | g $kg^{-1}$ | 149.3 | 132.3 | 48 | 153.7 | nd |
| dolomite | g $kg^{-1}$ | nd | 2.6 | nd | nd | nd |
| graphite | g $kg^{-1}$ | nd | 19.8 | nd | 36.1 | nd |
| hematite | g $kg^{-1}$ | 22.7 | 21.3 | 37.8 | 23.4 | nd |
| magnetite | g $kg^{-1}$ | 31.8 | 25 | 42 | 47 | nd |
| wüstite | g $kg^{-1}$ | 22.1 | 9.2 | 9.1 | 10.1 | nd |
| $\alpha$-iron | g $kg^{-1}$ | 4.8 | 1.3 | 1.5 | 5.3 | nd |
| kaolinite | g $kg^{-1}$ | 5.2 | 18.7 | 55.4 | nd | nd |
| muscovite | g $kg^{-1}$ | nd | nd | 62.2 | nd | nd |
| quartz | g $kg^{-1}$ | 22.1 | 63.2 | 213.8 | 27.3 | nd |

[a]The mineralogy was quantified by Rietveld refinement of conventional XRD data measured with Cu K$\alpha$ radiation. The "amorphous" material consists of coke and other amorphous or poorly crystalline phases. [b]Fresh BFS from the blast furnace Schwelgern 2 in Duisburg, Germany. [c]According to Munsell color charts. [d]$C_{carb}$ = carbonate carbon; $C_{noncarb}$ = total carbon minus carbonate carbon, includes organic carbon, graphite, and black carbon from coke.

was set to 13 085 eV, that is, 50 eV above the Pb $L_{III}$ absorption edge. On each sample, several points of interest (POIs) were selected for $\mu$-EXAFS (extended X-ray absorption fine structure) spectroscopy at the Zn K-edge (9659 eV). The selection of POIs for $\mu$-EXAFS was based on elemental distributions and correlations of Zn, Fe, Ca, and other elements, attempting to cover various types of spots, for example, well-defined Zn-rich hotspots and regions with lower Zn contents, respectively. $\mu$-EXAFS spectra were deadtime-corrected and averaged using in-house software tools developed at Beamline 10.3.2 and subsequently analyzed using Athena.[9,10]

**Bulk X-ray Absorption Spectroscopy.** XAS spectra of powdered BFS samples were collected at the Zn K-edge at Beamline 4-1 of the Stanford Synchrotron Radiation Light-source (SSRL, Stanford, CA). Powdered samples were uniformly packed into Al sample holders, sealed with Kapton tape, and measured in transmission mode at room temperature. The double crystal Si(220) monochromator was calibrated by setting the first inflection point of the absorption edge of a Zn-foil spectrum to 9659 eV. Higher harmonics were rejected using two mirrors placed before and after the monochromator.

Data reduction and linear combination fitting (LCF) of the XAS spectra was performed using Athena.[9,10] The selection of reference spectra for LCF was supported by principal component analysis (PCA) with subsequent target transformation (TT)[11,12] testing of a large set of Zn reference spectra available from previous studies.[13−17] Based on the PCA-TT (Table S1, Supporting Information) and preliminary LCF results, the following six Zn reference species (with their abbreviations given in parentheses) were selected for the final LCF analysis: (1 and 2) synthetic kerolite-type phyllosilicates synthesized with a Zn/(Zn + Mg) ratio of 0.25 (Zn25Clay) and 0.75 (Zn75Clay), respectively, (3) hydrozincite, $Zn_5(OH)_6(CO_3)_2$ (ZnHydro), (4) sphalerite (ZnS), (5) KZn−ferrocyanide ($K_2Zn_3[Fe(CN)_6]_2 \cdot 9H_2O$) (ZnCyan), and (6) Zn sorbed to ferrihydrite (ZnFh). Note, that Zn nitrate (dissolved, 0.5 M) was not included in the final LCF, despite the low SPOIL value, because it was never fitted as a significant component. Figure S3 of the Supporting Information shows the K-edge EXAFS spectra of the Zn reference compounds used in the final LCF and franklinite for comparison.

## RESULTS

**Elemental Composition and Mineralogy.** The chemical and mineralogical composition of selected BFS samples is reported in Table 1. Additional data for all samples analyzed by EXAFS spectroscopy in this study are provided in Table S2 (Supporting Information). In the following, we briefly summarize minimum and maximum values of chemical properties measured in up to $n$ = 36 BFS samples collected

at the Herne-Wanne site.[2] The BFS had neutral to alkaline pH values (pH 7.1−10.7; $n$ = 36) and contained significant amounts of carbonates, mainly consisting of calcite ($CaCO_3$). The BFS also contained high noncarbonate carbon contents (46−393 g $kg^{-1}$; $n$ = 32), including organic carbon, graphite, and black carbon, explaining the dark gray to black colors of many samples. The contents of Fe (40−241 g $kg^{-1}$; $n$ = 32), sulfur (2.4−15.8 g $kg^{-1}$; $n$ = 32), and cyanides (0.30−6.10 g $kg^{-1}$; $n$ = 36) were also high in most samples. The trace metal contents of the BFS were extremely high for Zn (15.7−86.4 g $kg^{-1}$; $n$ = 32), Pb (1.42−9.51 g $kg^{-1}$; $n$ = 32) and Cd (5.6−95.3 mg $kg^{-1}$; $n$ = 32). Overall, the chemical composition of the BFS from the Herne-Wanne site was comparable to values reported in the literature for other sites.[1,3]

The mineralogy of selected BFS samples, determined by Rietveld refinement of conventional powder XRD data, is also reported in Table 1. Very large fractions of the BFS were X-ray amorphous (432−798 g $kg^{-1}$; $n$ = 32), that is, they did not give rise to any distinct diffraction peaks and their constituents could therefore not be further identified by XRD. The dominating crystalline phases identified by XRD included (all $n$ = 32) calcite (48−208 g $kg^{-1}$), graphite (0−57 g $kg^{-1}$), hematite (9−109 g $kg^{-1}$), magnetite (10−57 g $kg^{-1}$), wüstite (3−49 g $kg^{-1}$), kaolinite (0−78 g $kg^{-1}$), and quartz (18−214 g $kg^{-1}$).

Since conventional XRD did not reveal any Zn-bearing mineral phases, we also collected synchrotron XRD patterns of the BFS (Figure 1; Figure S4, Supporting Information). The data indicated the presence of at least one of the two polymorphic ZnS phases wurtzite ($\alpha$-ZnS) and sphalerite ($\beta$-ZnS) in the fresh sample (BFS-2153) and in three samples from the Herne-Wanne site (C-2123; Figure 1). Since most of the main XRD peaks of both phases overlap, only wurtzite could be identified unambiguously by the peaks at 3.3 and 2.9 Å $d$-spacing, respectively (7.7 and 8.7 °2$\theta$ for $\lambda$ = 0.4432 Å), corresponding to the (100) and (101) planes. The peaks at 3.1, 1.9, and 1.6 Å (8.1, 13.3, and 15.6 °2$\theta$; Figure S4) can arise from both phases and could therefore not be assigned unambiguously. Similarly, the XRD peak at 2.7 Å (9.4 °2$\theta$), which is typically assigned to the sphalerite (200) reflection, overlaps widely with the hematite ($\bar{1}$14) reflection and could therefore not be used for sphalerite identification. Sphalerite and wurtzite typically occur together in spherical aggregates. Hence, our synchrotron XRD data indicate the presence of ZnS particles in some of the samples, containing wurtzite possibly intermixed with sphalerite. Additionally, five samples exhibited weak diffraction peaks (Figure 1) consistent with the phase potassium zinc hexacyanoferrate(II)−nonahydrate ($K_2Zn_3[Fe(CN)_6]_2 \cdot 9H_2O$).[6]

**Identification of Zn Species by $\mu$-XRF and $\mu$-EXAFS.** Elemental mapping by $\mu$-XRF combined with $\mu$-EXAFS spectroscopy on selected points of interest (POIs) can provide highly valuable information such as the spatial distribution of selected elements, spatial correlations between different elements, and potentially the unequivocal identification of minor Zn species in complex mixtures, which helps constraining the interpretation of bulk EXAFS spectra by linear combination fitting for quantitative Zn speciation.[13,18,19] Therefore, we shall first present and discuss the results of $\mu$-XRF and $\mu$-EXAFS, followed by a quantitative Zn speciation analysis based on bulk EXAFS spectroscopy.

Element distribution maps for Zn, Fe, and Ca obtained by synchrotron $\mu$-XRF analysis of a thin-sectioned BFS sample

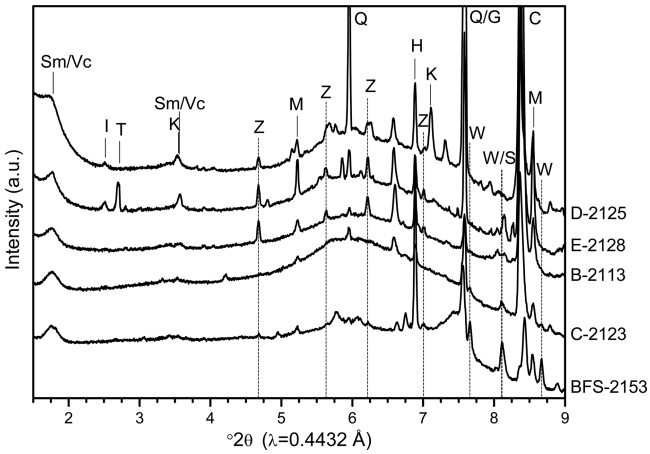


**Figure 1.** Synchrotron XRD patterns of selected BFS from ponds B−E of the former sedimentation pond site in Herne-Wanne and one fresh sludge sample (BFS-2153) from the blast furnace Schwelgern 2. The main peaks are labeled as follows: Q, quartz; C, calcite; H, hematite; M, magnetite; G, graphite; K, kaolinite; W, wurtzite; S, sphalerite; Z, KZn−cyanoferrate; I, Illite; Sm/Vc, smectite/vermiculite; T, talc. Detectable Zn-bearing minerals are marked with dashed lines (Z and W/S). The incoming X-ray energy was 27 973 eV.

(pond A) are presented in Figure 2. The maps were used to identify "hotspots" (i.e., spots with high concentration) for each element and possible spatial correlations between different elements of interest. Panels (a) and (c) in Figure 2 show two different regions on the sample, while panels (b) and (d) are fine maps of smaller areas (R1, R2) within each region scanned with higher spatial resolution.

All maps show clear hotspots of Zn, Fe, and Ca but no obvious spatial relationships between these elements. Also, no clear correlations between Zn and other measured elements (Ti, Cr, Mn, Ni, Cu, Pb) were observed. The most intense Zn hotspots appeared to be between 5 and 25 $\mu$m in diameter. Besides the Zn hotspots, significant amounts of Zn were also present in much smaller particles finely distributed throughout the samples. Region 2 exhibited a Ca-rich band separating an upper layer containing less Zn from a very Zn-rich layer below the Ca-rich band. A similar layering was also observed in region 1, although less pronounced. Also the spatial distribution of Fe and Ca exhibited hotspots of about 5−15 $\mu$m in diameter, as well as much smaller enrichments.

Based on elemental composition and morphology, eight POIs (Figure 2) on the sample were analyzed by Zn K-edge $\mu$-EXAFS spectroscopy. The spectra of five POIs that clearly differed from each other are presented in Figure 3, along with the corresponding linear combination fits. The LCF fitting results for all POIs are reported in Table 2, and the remaining $\mu$-EXAFS spectra are shown in Figure S5 of the Supporting Information.

The first spectrum shown in Figure 3 is from a POI (R1-3) representing the finely distributed Zn in the sample. The LCF results showed that the majority (74%) of the total Zn at this POI was bound in octahedral sheets of phyllosilicate structures (Table 2, sum of Zn25Clay and Zn75Clay). Smaller fractions of the total Zn were present as ZnS and tetrahedrally coordinated adsorbed Zn (fitted as ZnFh), respectively. Other POIs within the finely distributed Zn exhibited a very similar Zn speciation. One example is R1-6, with 78% Zn in clays, 10% in ZnS, and 9% adsorbed Zn. Another, somewhat similar example is R2-7,

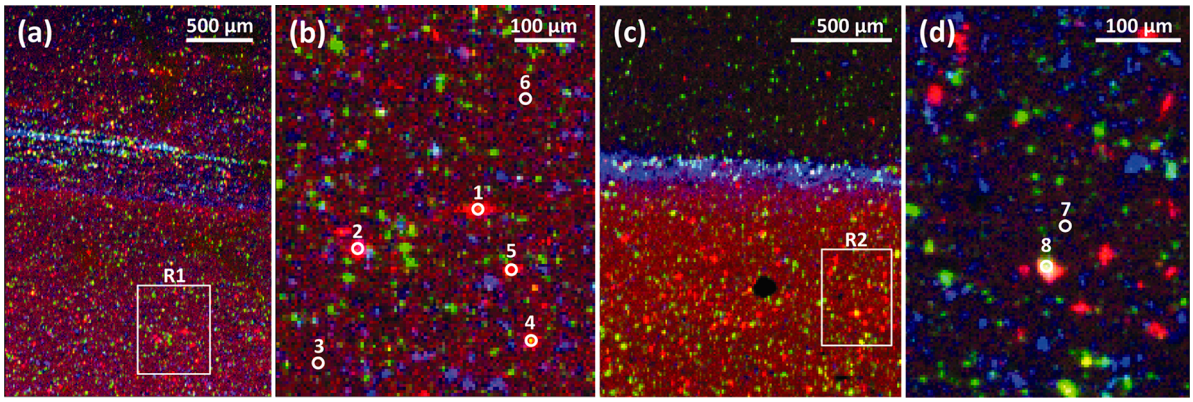


**Figure 2.** $\mu$-XRF tricolor elemental maps showing the distribution of Zn (red), Fe (green), and Ca (blue) in a BFS sample from pond A (~60 cm depth). (a, b) Coarse and fine maps of region 1 (R1) with POIs 1−6; (c, d) coarse and fine maps of region 2 (R2) with POIs 7 and 8.

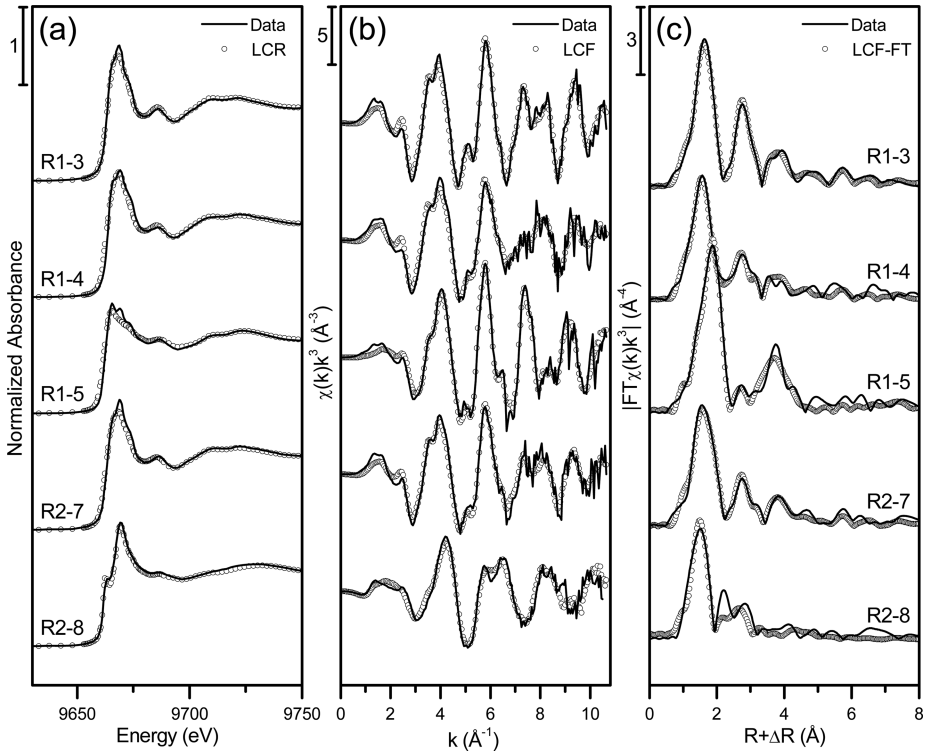


**Figure 3.** (a) Zn K-edge $\mu$-XANES, (b) $\mu$-EXAFS chi-functions, and (c) $\mu$-EXAFS Fourier transform magnitude functions (lines) of selected POIs (3−5 on R1; 7−8 on R2, see Figure 2). Symbols represent corresponding linear combination fits (LCF) for $\mu$-EXAFS spectra and linear combination reconstructions (LCR) based on the $\mu$-EXAFS fitting results for $\mu$-XANES spectra, respectively. LCF fits were done in k-space using a k-range of 3-11 $Å^{-1}$. The fitting results are reported in Table 2.

although this POI only had 46% Zn in clays and larger amounts of other Zn species.

The second spectrum in Figure 3 (R1-4), representing a Zn hotspot, which was also high in Fe, contained 60% Zn in clays, 23% adsorbed Zn (fitted as ZnFh), and 13% Zn in KZn−ferrocyanide, $K_2Zn_3[Fe(CN)_6]_2 \cdot 9H_2O$, which was previously identified by powder XRD.[6] Less than 5% of the total Zn at this POI was present as ZnS.

The third spectrum (R1-5) in Figure 3 was obtained from a very bright Zn hotspot that was strongly dominated by Zn in ZnS (62%). Minor species at this spot were Zn in phyllosilicates, hydrozincite, and adsorbed Zn, respectively. Another very similar spectrum with 73% ZnS was obtained from R1-2, also a very bright Zn hotspot. Spectrum R1-1 also contained 66% ZnS but together with 34% zincite (ZnO). This was the only spot at which ZnO was indicated. Also, ZnO was never accepted as a reference in LCF of bulk EXAFS spectra, suggesting that this Zn species was present only in minute traces.

The last spectrum (R2-8) in Figure 3 was clearly different from all others, both in the X-ray absorption near-edge structure (XANES) and the extended X-ray absorption fine structure (EXAFS) regions. It was best fitted with a KZn−ferrocyanide (ZnCyan) as the major species (51%), with 40% adsorbed Zn and only 5% Zn in clays and 4% in ZnS. This spectrum (both XANES and EXAFS) provided the strongest evidence for the existence of KZn−ferrocyanides in the BFS samples, which would be very difficult to attain by bulk-EXAFS alone.

**Table 2. Results of Linear Combination Fitting (LCF) of the $\mu$-EXAFS Spectra ($k$ = 3−11 Å$^{-1}$)**

| | % of total Zn (normalized to sum = 100)[b] | | | | | | | | |
|---|---|---|---|---|---|---|---|---|---|
| region POI[a] | Zn25Clay | Zn75Clay | ZnHydro | ZnS | ZnCyan | ZnFh | ZnO | fitted sum[c] (%) | NSSR[d] (%) |
| R1-1 | — | — | — | 66 | — | — | 34 | 106.3 | 8.44 |
| R1-2 | — | 9 | — | 73 | — | 18 | — | 114.0 | 5.04 |
| R1-3* | 25 | 49 | — | 16 | — | 10 | — | 100.0 | 3.94 |
| R1-4* | 42 | 18 | — | 4 | 13 | 23 | — | 110.4 | 10.53 |
| R1-5* | — | 13 | 9 | 62 | — | 16 | — | 114.6 | 5.86 |
| R1-6 | 33 | 45 | — | 10 | 3 | 9 | — | 108.7 | 3.58 |
| R2-7* | 23 | 23 | 15 | 18 | 9 | 12 | — | 108.3 | 9.05 |
| R2-8* | 5 | — | — | 4 | 51 | 40 | — | 99.4 | 15.77 |

[a]The locations of the analyzed spots (POI) on sample regions R1 and R2 are shown in Figure 2. The spectra for POIs marked with an asterisk are presented in Figure 3. [b]Abbreviations for the Zn reference species are Zn25Clay = synthetic 2:1 phyllosilicate with 25% Zn in the octahedral sheet; Zn75Clay = synthetic 2:1 phyllosilicate with 75% Zn in the octahedral sheet; ZnHydro = hydrozincite; ZnS = sphalerite; ZnCyan = KZn-ferrocyanide, ZnFh = Zn sorbed to ferrihydrite, and ZnO = zincite. [c]Fitted sum of all references before normalization. [d]Normalized sum of the squared residuals (NSSR (%) = $100\cdot\Sigma(\text{data}_i - \text{fit}_i)^2/\Sigma(\text{data}_i)^2$).

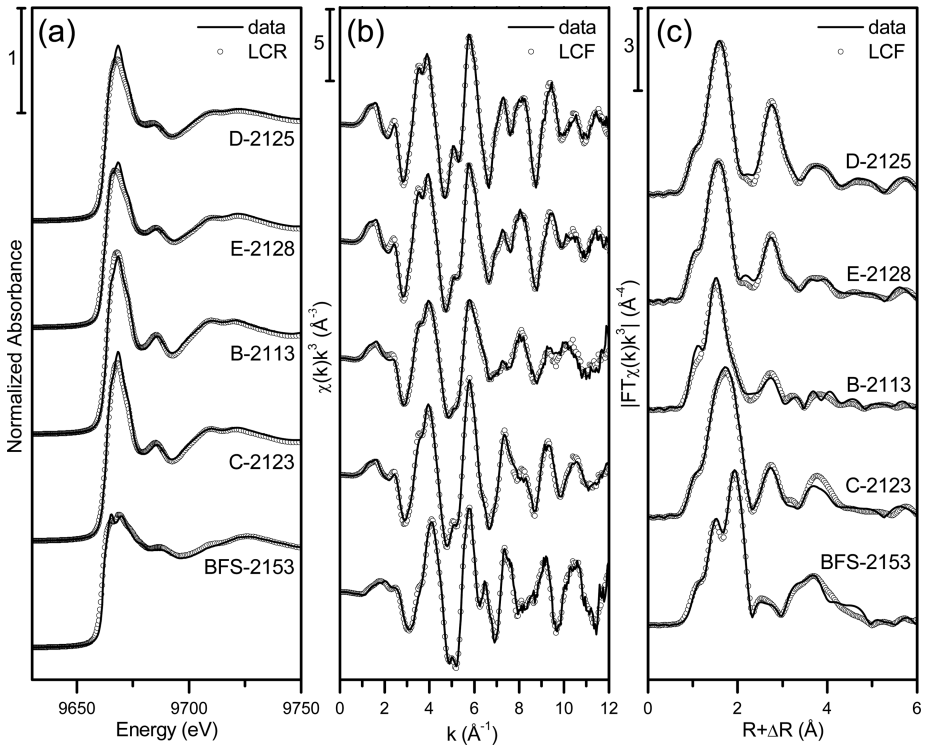


**Figure 4.** (a) Zn K-edge XANES, (b) EXAFS chi-functions, and (c) EXAFS Fourier transform magnitude functions of selected blast furnace sludge samples (lines). Symbols represent corresponding linear combination fits (LCF) for EXAFS spectra and linear combination reconstructions (LCR) based on the EXAFS fitting results for XANES spectra, respectively. LCF fits were done in k-space using a k-range of 3−12 Å$^{-1}$. The fitting results are reported in Table 3.

The measured XANES spectra (lines) presented in Figure 3a were well reconstructed (symbols) based on the normalized LCF fitting results of the corresponding EXAFS spectra. This provided additional confidence in the plausibility of the LCF results. Overall, the $\mu$-EXAFS data revealed that the finely divided Zn particles were dominated by Zn in the octahedral sheets of phyllosilicate minerals, while the bright Zn hotspots contained mainly ZnS or a KZn−ferrocyanide phase, previously identified as $K_2Zn_3[Fe(CN)_6]_2\cdot 9H_2O$.[6] Additionally, tetrahedrally coordinated adsorbed Zn (fitted as ZnFh) was found in almost all POIs, which is not surprising considering the high Fe and calcite contents of the BFS and the high pH values. Three of nine POIs also showed minor amounts of Zn in hydrozincite.

**Quantitative Zn Speciation by Bulk EXAFS.** The bulk XANES and EXAFS spectra of four selected BFS samples from different sedimentation ponds within the Herne-Wanne site and one fresh sample (BFS-2153) from an active blast furnace are presented in Figure 4, along with the corresponding LCF fits of the EXAFS spectra. The LCF fitting results are compiled in Table 3, and the remaining EXAFS spectra are shown in Figure S6 of the Supporting Information. PCA indicated five independent spectral components, which were used for target transformation testing of reference spectra (Table S1, Supporting Information). All reference spectra used in the final LCF had "good" SPOIL values (<3), except for Zn25Clay, which will be discussed later. The reference "Zn nitrate, dissolved" also had a low SPOIL value, but it was never

Table 3. Results of Linear Combination Fitting (LCF) of the Bulk EXAFS Spectra ($k$ = 3−12 Å$^{-1}$)

| BFS sample[a] | depth (cm) | % of total Zn (normalized to sum = 100)[b] | | | | | | fitted sum[d] (%) | NSSR[e] (%) |
|---|---|---|---|---|---|---|---|---|---|
| | | Zn25Clay | Zn75Clay | ZnHydro | ZnS[c] | ZnCyan[c] | ZnFh | | |
| A-2107 | 90−120 | 39 | 39 | 17 | 5 | — | — | 99.1 | 1.65 |
| A-2164 | 420−480 | 32 | 36 | 11 | 1 | 12 | 8 | 100.8 | 1.85 |
| A-2166 | 710−760 | 35 | 39 | 3 | 2 | 12 | 9 | 100.5 | 1.55 |
| B-2113* | 10−23 | 19 | 4 | 39 | 8 | + 11 | 19 | 97.9 | 4.40 |
| B-2115 | 36−120 | 35 | 18 | 34 | 2 | 7 | 4 | 101.1 | 2.49 |
| C-2116 | 0−45 | 20 | 28 | 16 | (+) 23 | — | 13 | 100.4 | 1.55 |
| C-2117 | 45−120 | 23 | 12 | 20 | (+) 36 | — | 9 | 106.4 | 1.34 |
| C-2123* | 85−120 | 20 | 19 | 24 | (+) 32 | — | 5 | 102.8 | 1.40 |
| D-2125* | 60−120 | 35 | 42 | 20 | 3 | (+) — | — | 93.6 | 1.23 |
| D-2189 | 565−595 | 33 | 55 | — | 3 | — | 9 | 90.3 | 7.44 |
| E-2128* | 80−120 | 44 | 22 | 21 | 1 | + 5 | 7 | 97.9 | 1.35 |
| F-2131 | 61−120 | 26 | 49 | 23 | 2 | (+) — | — | 93.6 | 1.42 |
| BFS-2153* | — | 7 | — | — | + 50 | (+) 24 | 18 | 107.3 | 2.27 |

[a]The sample code represents the sedimentation pond (A−F) and the sample number. BFS-2153 is a fresh sludge from the blast furnace Schwelgern 2 in Duisburg, Germany. Spectra of samples marked with an asterisk are presented in Figure 4. [b]Abbreviations for the Zn reference species are: Zn25Clay = synthetic 2:1 phyllosilicate with 25% Zn in the octahedral sheet; Zn75Clay = synthetic 2:1 phyllosilicate with 75% Zn in the octahedral sheet; ZnHydro = hydrozincite; ZnS = sphalerite; ZnCyan = KZn-ferrocyanide, and ZnFh = Zn sorbed to ferrihydrite [c]Prefix "+": ZnS or KZn−ferrocyanide were detected by synchrotron XRD; "(+)": the diffraction peaks were extremely weak. [d]Fitted sum of all references before normalization. [e]eNormalized sum of the squared residuals (NSSR (%) = $100 \cdot \Sigma(\text{data}_i - \text{fit}_i)^2/\Sigma(\text{data}_i)^2$).

accepted in the preliminary fits as significant contribution and therefore dropped.

The first sample (D-2125) was strongly dominated by Zn in phyllosilicates (77%), with smaller amounts of Zn in hydrozincite (20%) and traces of ZnS. Also, the second sample (E-2128) was dominated by Zn in phyllosilicates (66%), although it contained somewhat larger contents of other species including Zn in hydrozincite (21%), adsorbed Zn (7%), and small amounts of Zn in KZn−ferrocyanide (5%). The third spectrum (B-2113) showed a mix of Zn in hydrozincite (39%), Zn in phyllosilicates (23%), adsorbed Zn (19%), Zn in KZn−ferrocyanide (11%), and in ZnS (8%). The fourth spectrum (C-2123) exhibited a strong ZnS component (32%) and also contained considerable amounts of Zn in phyllosilicates (39%) and in hydrozincite (24%), besides small amounts of adsorbed Zn (5%). The last spectrum in Figure 4 (BFS-2153) is from a fresh BFS that had not been deposited in sedimentation ponds. It was strongly dominated by Zn in ZnS (50%) but also indicated Zn in KZn−ferrocyanide (24%), adsorbed Zn (18%), and minor amounts of Zn in octahedral sheets of clay minerals (7%).

In summary, the BFS from the Herne-Wanne site contained strongly variable amounts of Zn in the octahedral sheets of phyllosilicates (23−88%), Zn in ZnS (1−36%), Zn in a KZn−ferrocyanide phase (0−12%), Zn in hydrozincite (0−39%), and tetrahedrally coordinated adsorbed Zn (0−19%), respectively. The minerals franklinite ($ZnFe_2O_4$), zincite (ZnO), and smithsonite ($ZnCO_3$) were not detected by bulk EXAFS.

## DISCUSSION

**Zn Speciation in BFS.** With the exception of polymorphs of ZnS (wurtzite and possibly sphalerite) and a KZn−ferrocyanide phase ($K_2Zn_3[Fe(CN)_6]_2 \cdot 9H_2O$), no other crystalline Zn compounds could be detected in the BFS from the Herne-Wanne site by conventional and synchrotron XRD. The diffraction peaks of these phases were always very weak, if detected at all. This is consistent with previous reports, in which no or only traces of crystalline Zn phases were detected in BFS by XRD.[1,3,20] Additionally, quantification of these phases by XRD is impossible due to their small contents (<3% of the total mass) and the extremely high fractions of X-ray amorphous materials in the BFS (Table 1).

With the combination of bulk- and microfocused XRF and EXAFS analyses, we identified five major types of Zn species and quantified their relative contributions in 12 BFS samples from the Herne-Wanne site and one fresh sample from another blast furnace. In the following paragraphs, we shall briefly discuss each of the five types of Zn species.

The dominant Zn species, occurring in rather large amounts in all BFS from the sedimentation pond site, was Zn in phyllosilicates, in which Zn occupies central cation positions within the octahedral sheets, together with other elements such as Mg or Al. For LCF of the BFS spectra, we used the Zn25Clay instead of the Zn50Clay, although the latter returned a lower SPOIL value in PCA-TT analysis (Table S1, Supporting Information). Figure S7b of the Supporting Information demonstrates that the spectrum of Zn50Clay was perfectly fitted with a linear combination of Zn25Clay and Zn75Clay in a 1:1 ratio. Thus, Zn50Clay is not an independent reference and can be dropped from LCF analysis if Zn25Clay and Zn75Clay are included in the analysis. Since the Zn contents of phyllosilicate phases in the BFS samples were *a priori* unknown and may vary considerably, we considered this fitting approach superior, because it accounts for phyllosilicates with 25−75% Zn in the octahedral positions. From the fitted fractions of Zn25clay and Zn75clay (Table 3), we estimated that the Zn-bearing phyllosilicates in the deposited BFS had 35−58% of their octahedral sites occupied with Zn.

The incorporation of Zn into the octahedral sheets of claylike precipitates has been widely observed to occur in neutral to alkaline soils, especially in highly contaminated soils affected by smelter emissions[21,22] or soils contaminated by Zn emissions from corroding galvanized steel.[14] In agreement with these field studies, laboratory experiments in which $Zn^{2+}$ was equilibrated with aluminosilicate minerals over periods from days to weeks under neutral to alkaline pH conditions have also confirmed the incorporation of Zn into the octahedral sheets of LDH or phyllosilicate minerals.[23,24] Although these two types of layered

Zn species are not easily distinguished by bulk EXAFS, the spectra of our BFS samples more closely resembled those of Zn in clay minerals rather than Zn in LDH structures. The most prominent features differentiating these two types of minerals are illustrated in Figure S8 of the Supporting Information. However, we cannot exclude the coexistence of Zn in LDH phases alongside with Zn in clay minerals. In fact, when we included Zn-LDH as another possible reference species in LCF, most samples were fitted with a mixture of Zn in LDH and clays, with an average of 32 ± 23% of the total octahedral Zn in layered minerals in LDH at the cost of Zn in phyllosilicates.

The presence of ZnS in BFS was also reported in previous studies.[1,3] Our quantitative Zn speciation by EXAFS analysis suggested between 1% and 36% of the total Zn was present as ZnS, which corresponded to ZnS contents between 0.02% and 2.2% of the sample mass. ZnS was detected by synchrotron XRD as wurtzite ($\alpha$-ZnS), possibly with additional sphalerite ($\beta$-ZnS), in the four samples with the highest ZnS contents (1.3−2.2% ZnS), but was undetectable by XRD in all other samples (Table 3). Both ZnS phases cannot be distinguished from each other by EXAFS spectroscopy, because their spectra are too similar. The ZnS content determined by EXAFS correlated with the total S content of the BFS (Figure 5a). Samples with less than 5 g $kg^{-1}$ total S generally had low ZnS contents, whereas the highest ZnS contents were found in the samples with the highest total S contents (11−16 g $kg^{-1}$). However, all samples contained significantly more S than could be theoretically bound in ZnS (Figure 5a), suggesting the presence of other metal sulfides (e.g., PbS) or oxidized sulfur species.

As shown in Figure 5b, there was also a correlation between the amounts of Zn in Zn−cyanides and the total CN content of the BFS. In this case, the data scatter around the theoretical stoichiometry line of KZn−ferrocyanide $K_2Zn_3[Fe(CN)_6]_2 \cdot 9H_2O$, which was previously identified by XRD.[6] This suggests that this cyanide phase may indeed be the main form of cyanide in the BFS samples, as previously speculated by Dohrmann and Mansfeldt.[25]

The presence of hydrozincite in the BFS is consistent with a recent study by Jacquat et al.,[14] who showed that this phase forms as crusts around limestone particles in calcareous, highly Zn-contaminated soils. These authors also calculated that hydrozincite formation is thermodynamically more favorable at atmospheric or elevated $CO_2$ partial pressure than formation of zincite (ZnO) and smithsonite ($ZnCO_3$), which were both not detected in the soils. Similarly, we did not detect these Zn phases in our samples (except for ZnO at POI R1-1), which were sometimes assumed to be present in BFS without analytical proof.

The Zn fractions fitted with the ZnFh (Zn sorbed to ferrihydrite) reference represents primarily tetrahedrally coordinated Zn sorbed as inner-sphere complexes, whereby poorly crystalline iron oxyhydroxides were presumably the most important sorbents. In addition to 1−11% ($n$ = 32) of hematite detected by XRD/Rietveld analysis (see Table 1 for examples), it is likely that the BFS also contained significant amounts of high surface area, low-crystallinity iron oxyhydroxides that were not identified by XRD. It is well known that Zn forms strong inner-sphere surface complexes on ferrihydrite at neutral to alkaline pH,[26−28] and therefore, this Zn species is also geochemically very plausible. However, the presence of tetrahedrally coordinated Zn sorbed to calcite may also contribute to this fitted fraction.

Another Zn mineral species, which was previously reported to occur in BFS,[1] is franklinite ($ZnFe_2O_4$), a spinel-group mineral that was found to be a major species in acidic, smelter-affected soils.[15] However, this phase was not detected in any of our BFS samples by XRD or EXAFS, despite its very pronounced and characteristic oscillations in the EXAFS region (Figure S3, Supporting Information). If only a few percent of the total Zn were present as franklinite, we would expect a clear signal in the EXAFS spectra. We can therefore exclude franklinite as an important Zn species in the BFS of the Herne-Wanne site.

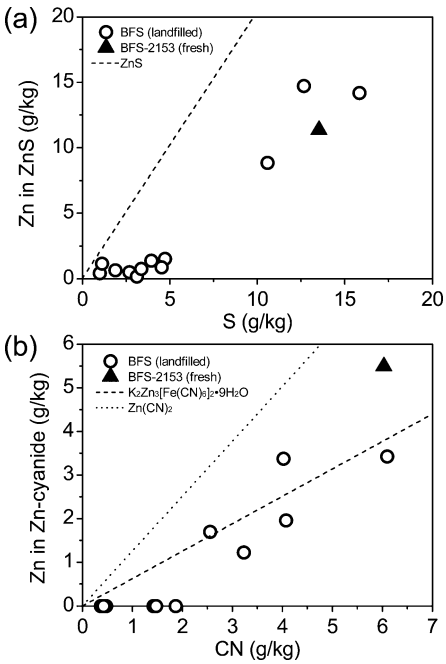


**Figure 5.** Correlations between (a) the total S content and the amounts of Zn bound in ZnS, and (b) the total CN content and the amounts of Zn bound in KZn−ferrocyanide. Total S was determined by XRF analysis, total CN by microdistillation, and Zn species by bulk EXAFS spectroscopy and LCF. The dashed lines indicate stoichiometric ratios between (a) Zn and S in ZnS and (b) Zn and CN in either $K_2Zn_3[Fe(CN)_6]_2 \cdot 9H_2O$ or $Zn(CN)_2$, respectively.

**Weathering-Induced Changes in Zn Speciation.** The comparison of the deposited BFS with the fresh sample (BFS-2153), which contained little Zn in phyllosilicates and no detectable hydrozincite, may lead to the hypothesis that these Zn species have formed after deposition by weathering and mineral transformation processes. Unfortunately, it was not possible to compare deposited and fresh BFS from the same blast furnace, and therefore, we cannot corroborate this hypothesis. Additional studies are required to investigate weathering processes and mineral transformations in deposited BFS.

Voegelin et al.[17] demonstrated that oxidative ZnS weathering in soils was favored by neutral to alkaline pH conditions and that the released Zn was incorporated into secondary Zn-LDH and/or phyllosilicate structures, as well as adsorbed, tetrahedrally coordinated Zn species. Similar redox-induced changes in Zn speciation have also been reported along depth profiles in a floatation residue deposit near a former Zn/Pb sulfide mine.[16] However, in our study, the Zn speciation within the sampled ponds was depth-independent, while much larger differences in

Zn speciation were observed between the ponds (Table 3). Therefore, we suggest that postdepositional weathering and mineral transformation processes were probably not induced by leaching or vertical redox gradients. Instead, secondary Zn species, such as Zn-bearing phyllosilicates and/or hydrozincite, may have formed shortly after the BFS were deposited into the sedimentation ponds of the Herne-Wanne site. The observed variations in Zn speciation between ponds may reflect differences in the original BFS composition, which may have varied during the period of pig iron production.

## ENVIRONMENTAL IMPLICATIONS

We identified 5 major types of Zn species in BFS and quantified their abundance in 12 samples from a former BFS sedimentation pond site. The speciation of Zn and other trace metals is of great importance for predicting the potential mobility of the metals with water leaching to groundwater or surface water bodies. Zn released by oxidative ZnS weathering will most likely be bound as Zn in phyllosilicate minerals, Zn adsorbed inner-spherically to iron oxyhydroxides, and/or Zn in hydrozincite, respectively. Thus, the leaching potential of Zn from the sedimentation pond site is expected to be low as long as the pH values remain in the neutral to weakly alkaline range. Several recent studies have suggested the potential use of BFS for industrial wastewater treatment, especially the removal of trace metals such as Zn, Cd, Pb, and others, even though these materials are already enriched in these metals.[29,30] Our results suggest that Zn in wastewater may be incorporated into newly formed phyllosilicate or hydrozincite phases when reacted with BFS. Some other trace metals such as Ni and Co are expected to exhibit a similar behavior.

The speciation of Zn in BFS is also of great importance for the future development of improved hydrometallurgical methods for recovery of the Zn, which is a necessary prerequisite for the recycling of BFS to the blast furnace. The solubility of Zn, and therefore its extractability in acids and oxidizing solutions, strongly depends on Zn speciation.[14] Phases such as hydrozincite and Zn sorbed to iron oxyhydroxides are expected to be extractable under mildly acidic conditions, while the extraction of Zn in clay minerals and Zn–cyanides may require more strongly acidic conditions. The dissolution of ZnS requires oxidizing acidic conditions.[1,31] In the future, Zn and Fe recovery from BFS will gain importance due to environmental and economic factors.

## ASSOCIATED CONTENT

### Supporting Information

Additional information on the sampling site, elemental composition, XRD, and EXAFS analyses of the BFS. This material is available free of charge via the Internet at http://pubs.acs.org.

## AUTHOR INFORMATION

### Corresponding Author

*Phone: +41 44 6336003; fax: +41 44 6331118; e-mail: kretzschmar@env.ethz.ch.

### Notes

The authors declare no competing financial interest.

## ACKNOWLEDGMENTS

We gratefully acknowledge Josef Küper, City of Herne, for providing access to the field site, Dr. Rainer Dohrmann for conducting laboratory XRD/Rietveld analyses, Dr. Olivier Jacquat for help with building the Zn reference spectra database, and Dr. Christian Mikutta for support at SSRL beamline 4-1. Bulk XAS spectra were measured at the Stanford Synchrotron Radiation Lightsource (SSRL), a Directorate of SLAC National Accelerator Laboratory and an Office of Science User Facility operated for the U.S. Department of Energy Office of Science by Stanford University. $\mu$-XRF/XAS analyses were carried out at the Advanced Light Source (ALS). The ALS is supported by the Director, Office of Science, Office of Basic Energy Sciences, Material Sciences Division, of the U.S. Department of Energy under contract no. DE-AC03-76SF00098 at Lawrence Berkeley National Laboratory. Synchrotron XRD was performed at the Swiss Light Source, Paul Scherrer Institute, Villigen, Switzerland. Most reference spectra were collected during previous studies at the synchrotron ANKA. We are grateful to all machine and beamline groups whose outstanding efforts have made these experiments possible. This research project was financially supported by the Swiss National Science Foundation under grants nos. 200021-101876 and 200020-116592.

## REFERENCES

(1) Van Herck, P.; Vandecasteele, C.; Swennen, R.; Mortier, R. Zinc and lead removal from blast furnace sludge with a hydrometallurgical process. *Environ. Sci. Technol.* **2000**, *34* (17), 3802–3808.

(2) Mansfeldt, T.; Dohrmann, R. Chemical and mineralogical characterization of blast-furnace sludge from an abandoned landfill. *Environ. Sci. Technol.* **2004**, *38* (22), 5977–5984.

(3) Trung, Z. H.; Kukurugya, F.; Takacova, Z.; Orac, D.; Laubertova, M.; Miskufova, A.; Havlik, T. Acidic leaching both of zinc and iron from basic oxygen furnace sludge. *J. Hazard. Mater.* **2011**, *192* (3), 1100–1107.

(4) Das, B.; Prakash, S.; Reddy, P. S. R.; Misra, V. N. An overview of utilization of slag and sludge from steel industries. *Resour., Conserv. Recycl.* **2007**, *50* (1), 40–57.

(5) Steuer, J. Behandlung der Gichtgas-Waschwässer von Hochöfen – Optimierung der betrieblichen Wasserwirtschaft durch neue und kostengünstige Verfahrenstechniken unter besonderer Berücksichtigung des Wasser- und Rohstoffrecyclings sowie der Gewässerentlastung und der Abfallbeseitigung. Ph.D. dissertation, Rheinisch-Westfälische Technische Hochschule Aachen, Germany, 1986.

(6) Mansfeldt, T.; Dohrmann, R. Identification of a crystalline cyanide-containing compound in blast furnace sludge deposits. *J. Environ. Qual.* **2001**, *30* (6), 1927–1932.

(7) Mansfeldt, T.; Biernath, H. Method comparison for the determination of total cyanide in deposited blast furnace sludge. *Anal. Chim. Acta* **2001**, *435* (2), 377–384.

(8) Marcus, M. A.; MacDowell, A. A.; Celestre, R.; Manceau, A.; Miller, T.; Padmore, H. A.; Sublett, R. E. Beamline 10.3.2 at ALS: A hard X-ray microprobe for environmental and materials sciences. *J. Synchrotron Radiat.* **2004**, *11*, 239–247.

(9) Ravel, B.; Newville, M. ATHENA and ARTEMIS: Interactive graphical data analysis using IFEFFIT. *Phys. Scr.* **2005**, *T115*, 1007–1010.

(10) Ravel, B.; Newville, M. ATHENA, ARTEMIS, HEPHAESTUS: Data analysis for X-ray absorption spectroscopy using IFEFFIT. *J. Synchrotron Radiat.* **2005**, *12*, 537–541.

(11) Ressler, T.; Wong, J.; Roos, J.; Smith, I. L. Quantitative speciation of Mn-bearing particulates emitted from autos burning (methylcyclopentadienyl)manganese tricarbonyl-added gasolines using XANES spectroscopy. *Environ. Sci. Technol.* **2000**, *34* (6), 950–958.

(12) Beauchemin, S.; Hesterberg, D.; Beauchemin, M. Principal component analysis approach for modeling sulfur K-XANES spectra of humic acids. *Soil Sci. Soc. Am. J.* **2002**, *66* (1), 83–91.

(13) Jacquat, O.; Voegelin, A.; Juillot, F.; Kretzschmar, R. Changes in Zn speciation during soil formation from Zn-rich limestones. *Geochim. Cosmochim. Acta* **2009**, *73* (19), 5554−5571.
(14) Jacquat, O.; Voegelin, A.; Villard, A.; Marcus, M. A.; Kretzschmar, R. Formation of Zn-rich phyllosilicate, Zn-layered double hydroxide and hydrozincite in contaminated calcareous soils. *Geochim. Cosmochim. Acta* **2008**, *72* (20), 5037−5054.
(15) Roberts, D. R.; Scheinost, A. C.; Sparks, D. L. Zinc speciation in a smelter-contaminated soil profile using bulk and microspectroscopic techniques. *Environ. Sci. Technol.* **2002**, *36* (8), 1742−1750.
(16) Schuwirth, N.; Voegelin, A.; Kretzschmar, R.; Hofmann, T. Vertical distribution and speciation of trace metals in weathering flotation residues of a zinc/lead sulfide mine. *J. Environ. Qual.* **2007**, *36* (1), 61−69.
(17) Voegelin, A.; Jacquat, O.; Pfister, S.; Barmettler, K.; Scheinost, A. C.; Kretzschmar, R. Time-dependent changes of zinc speciation in four soils contaminated with zincite or sphalerite. *Environ. Sci. Technol.* **2011**, *45* (1), 255−261.
(18) Isaure, M.-P.; Laboudigue, A.; Manceau, A.; Sarret, G.; Tiffreau, C.; Trocellier, P.; Lamble, G.; Hazemann, J.-L.; Chateigner, D. Quantitative Zn speciation in a contaminated dredged sediment by $\mu$-PIXE, $\mu$-SXRF, EXAFS spectroscopy and principal component analysis. *Geochim. Cosmochim. Acta* **2002**, *66* (9), 1549−1567.
(19) Sarret, G.; Balesdent, J.; Bouziri, L.; Garnier, J.-M.; Marcus, M. A.; Geoffroy, N.; Panfili, F.; Manceau, A. Zn speciation in the organic horizon of a contaminated soil by micro-X-ray fluorescence, micro- and powder-EXAFS spectroscopy, and isotopic dilution. *Environ. Sci. Technol.* **2004**, *38* (10), 2792−2801.
(20) Vereš, J.; Jakabský, S.; Šepelák, V. Chemical, physical, morphological and structural characterization of blast furnace sludge. *Diffus. Fundam.* **2010**, *12*, 88−91.
(21) Manceau, A.; Lanson, B.; Schlegel, M. L.; Hargé, J. C.; Musso, M.; Eybert-Bérard, L.; Hazemann, J.-L.; Chateigner, D.; Lamble, G. M. Quantitative Zn speciation in smelter-contaminated soils by EXAFS spectroscopy. *Am. J. Sci.* **2000**, *300* (4), 289−343.
(22) Manceau, A.; Marcus, M. A.; Tamura, N.; Proux, O.; Geoffroy, N.; Lanson, B. Natural speciation of Zn at the micrometer scale in a clayey soil using X-ray fluorescence, absorption, and diffraction. *Geochim. Cosmochim. Acta* **2004**, *68* (11), 2467−2483.
(23) Schlegel, M. L.; Manceau, A.; Charlet, L.; Chateigner, D.; Hazemann, J.-L. Sorption of metal ions on clay minerals. III. Nucleation and epitaxial growth of Zn phyllosilicate on the edges of hectorite. *Geochim. Cosmochim. Acta* **2001**, *65* (22), 4155−4170.
(24) Schlegel, M. L.; Manceau, A. Evidence for the nucleation and epitaxial growth of Zn phyllosilicate on montmorillonite. *Geochim. Cosmochim. Acta* **2006**, *70* (4), 901−917.
(25) Dohrmann, R.; Mansfeldt, T. The chemical binding of cyanides in deposited blast furnace sludge. In *Applied Mineralogy in Research, Economy, Technology, Ecology and Culture*; Rammlmair, D., Mederer, J., Oberthür, T., Heimann, R. B., Pentinghaus, H., Eds.; A. A. Balkema: Rotterdam/Brookfield, The Netherlands, 2000; Vol. 2, pp 523−526.
(26) Lee, S.; Anderson, P. R. EXAFS study of Zn sorption mechanisms on hydrous ferric oxide over extended reaction time. *J. Colloid Interface Sci.* **2005**, *286* (1), 82−89.
(27) Waychunas, G. A.; Fuller, C. C.; Davis, J. A. Surface complexation and precipitate geometry for aqueous Zn(II) sorption on ferrihydrite: I. X-ray absorption extended fine structure spectroscopy analysis. *Geochim. Cosmochim. Acta* **2002**, *66* (7), 1119−1137.
(28) Waychunas, G. A.; Fuller, C. C.; Davis, J. A.; Rehr, J. J. Surface complexation and precipitate geometry for aqueous Zn(II) sorption on ferrihydrite: II. XANES analysis and simulation. *Geochim. Cosmochim. Acta* **2003**, *67* (5), 1031−1043.
(29) Lopez-Delgado, A.; Perez, C.; Lopez, F. A. Sorption of heavy metals on blast furnace sludge. *Water Res.* **1998**, *32* (4), 989−996.
(30) Lopez, F. A.; Perez, C.; Lopez-Delgado, A. The adsorption of copper(II) ions from aqueous solution on blast furnace sludge. *J. Mater. Sci. Lett.* **1996**, *15* (15), 1310−1312.
(31) Van Herck, P.; Vandecasteele, C. Evaluation of the use of a sequential extraction procedure for the characterization and treatment of metal containing solid waste. *Waste Manage.* **2001**, *21* (8), 685−694.

***Supporting Information to:***

# Speciation of Zn in blast furnace sludge from former sedimentation ponds using synchrotron X-ray diffraction, fluorescence, and absorption spectroscopy

Ruben Kretzschmar[1,*], Tim Mansfeldt[2], Petar N. Mandaliev[1], Kurt Barmettler[1], Matthew A. Marcus[3] , and Andreas Voegelin[1,4]

[1] *Institute of Biogeochemistry and Pollutant Dynamics, ETH Zurich, CHN, 8092 Zurich, Switzerland.*

[2] *Soil Geography/Soil Science, Department of Geosciences, University of Cologne, Albertus-Magnus-Platz, D-50923 Köln, Germany*

[3] *Advanced Light Source, Lawrence Berkeley National Laboratory, 1 Cyclotron Road, Berkeley, CA 94720, USA*

[4] *Eawag, Swiss Federal Institute of Aquatic Science and Technology, Überlandstrasse 133, CH-8600 Dübendorf, Switzerland.*

* Corresponding author phone: +41 44 6336003; fax: +41 44 6331118, E-mail: kretzschmar@env.ethz.ch

Contents:

Figure S1: Aerial photograph of the sampling site with the ponds and sampling locations marked.

Figure S2: Photo of sampling pit in pond A.

Table S1: Results of target transformation (TT) using the first 5 components from PCA of 13 bulk EXAFS spectra.

Table S2: pH and elemental composition of all BFS samples analyzed by EXAFS spectroscopy.

Figure S3: Zn K-edge XANES and EXAFS spectra of relevant Zn reference compounds.

Figure S4: Synchrotron XRD patterns of selected BFS samples (same as in Figure 1) over a different °2θ range.

Figure S5: Micro-EXAFS spectra and linear combination fits of all POIs not shown in Figure 3.

Figure S6: Bulk EXAFS spectra and linear combination fits of all BFS samples not shown in Figure 4.

Figure S7: Zn K-edge EXAFS spectra of synthetic Zn clays with different Zn contents.

Figure S8: Zn K-edge EXAFS spectra of a BFS sample (A-2107), Zn in a clay mineral structure, and Zn in ZnAl-LHD.

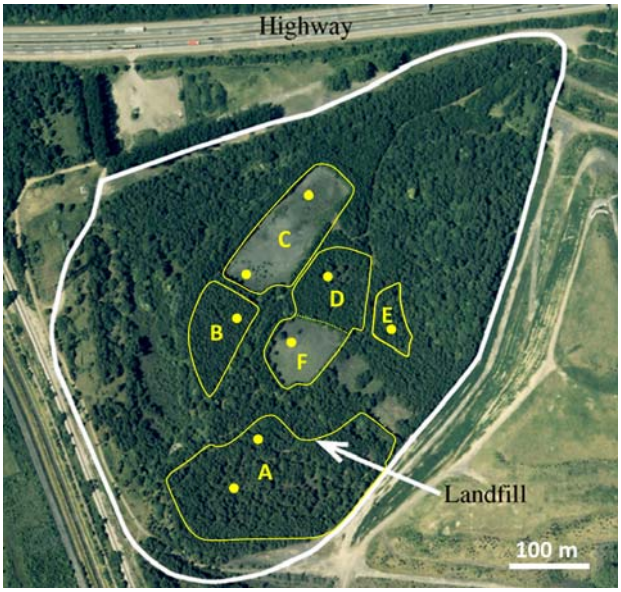


Figure S1. Aerial photograph of the former sedimentation pond site in Herne-Wanne, Germany, taken in the late 1989.[1] The yellow lines mark the ponds A-F and the yellow points the approximate sampling locations.

Figure S2. Soil profile in Pond A showing the layered BFS sediments with gray to black colors. The scale bar is divided into 10 cm sections.

Table S1. Results of target transformation (TT) using the first 5 components obtained from PCA with 13 bulk-EXAFS spectra ($k^3$-weighted chi-spectra, k-range 2 to 11 $Å^{-1}$). Zn references used in the final LCF analysis are marked by an asterisk.

| Zn reference spectrum | Publication [b] | SPOIL | LCF |
|---|---|---|---|
| ZnS (sphalerite, Alfa Aesar 40091) | 2 | 1.56 | * |
| ZnCyan ($K_2Zn_3[Fe(CN)_6]_2 \cdot 9H_2O$, synthesized) | | 1.70 | * |
| Zn nitrate, dissolved (0.5 M) | 3 | 2.04 | |
| Zn75Clay (kerolite, synthesized with Zn/(Zn+Mg)=0.75) | 3 | 2.32 | * |
| ZnFh (Zn sorbed to ferrihydrite, synthesized) | 3 | 2.53 | * |
| Zn50Clay (kerolite, synthesized with Zn/(Zn+Mg)=0.50) | 3 | 2.77 | |
| ZnHydro (hydrozincite, Alfa Aesar 33398) | 3 | 2.88 | * |
| Hemimorphite ($Zn_4Si_2O_7(OH)_2 \cdot H_2O$) | | 3.10 | |
| Smithsonite ($ZnCO_3$) | 3 | 4.14 | |
| ZnAl-LDH | 3 | 5.15 | |
| Zincite (ZnO, Merck 1.08849.0500) | 4 | 5.18 | |
| Zn hydroxide ($\alpha$-$Zn(OH)_2$) | 3 | 5.48 | |
| Zn in calcite ($ZnCaCO_3$, 1500 ppm Zn) | 3 | 5.64 | |
| Zn25Clay (kerolite, synthesized with Zn/(Zn+Mg)=0.25) | 3 | 5.69 | * |
| Zn in ferrihydrite (coprecipitate, 2% Zn) | 5 | 6.07 | |
| Franklinite ($ZnFe_2O_4$) | 6 | 10.06 | |
| Zn metal (foil) | | 17.44 | |

[a] Classification of SPOIL values according to Malinowski [7]: 0-1.5=excellent, 1.5-3=good, 3-4.5=fair, 4.5-6=acceptable, >6=unacceptable.
[b] Details about published references can be found in the cited publications. The hemimorphite sample was kindly provided by Maarten Nachtegaal (SLS, Paul Scherrer Institute).

Table S2: pH and elemental composition of all blast furnace sludge samples analyzed by EXAFS spectroscopy. Samples from greater than 2 m depth were taken with a coring device.

| Sample [a] | Depth | pH | Fe | Al | Si | Ca | Mg | K | S | CN | Zn |
|---|---|---|---|---|---|---|---|---|---|---|---|
| | cm | | g $kg^{-1}$ | | | | | | | | |
| A-2107 | 90-120 | 8.6 | 137.3 | 29.1 | 53.8 | 94.8 | 28.2 | 3.49 | 4.72 | 0.48 | 29.5 |
| A-2164 | 420-480 | 9.9 | 64.8 | 39.4 | 90.5 | 133.4 | 14.1 | 36.4 | 1.02 | 6.10 | 28.8 |
| A-2166 | 710-760 | 9.6 | 59.3 | 40.3 | 95.3 | 133.5 | 14.9 | 38.0 | 1.89 | 4.03 | 27.3 |
| B-2113 | 10-23 | 8.2 | 113.7 | 44.0 | 100.4 | 105.6 | 16.9 | 14.19 | 3.94 | 4.08 | 17.6 |
| B-2115 | 36-120 | 8.7 | 184.4 | 33.3 | 55.7 | 73.7 | 16.6 | 9.05 | 2.69 | 2.56 | 26.0 |
| C-2116 | 0-45 | 8.2 | 69.3 | 32.3 | 69.9 | 61.8 | 11.2 | 5.81 | 10.59 | 1.45 | 37.9 |
| C-2117 | 45-120 | 7.7 | 40.3 | 30.3 | 60.9 | 44.3 | 13.4 | 6.72 | 15.63 | 0.37 | 45.3 |
| C-2123 | 85-120 | 7.8 | 79.3 | 33.6 | 69.5 | 63.6 | 10.4 | 7.55 | 15.84 | 1.43 | 44.4 |
| D-2125 | 60-120 | 7.1 | 132.6 | 27.8 | 135.6 | 36.7 | 9.0 | 3.98 | 4.55 | 1.87 | 25.8 |
| D-2189 | 565-595 | 10.7 | 135.2 | 32.0 | 71.4 | 108.7 | 16.8 | 21.7 | 1.13 | 0.42 | 35.8 |
| E-2128 | 80-120 | 8.4 | 185.5 | 37.5 | 81.8 | 83.2 | 19.7 | 9.88 | 3.13 | 3.23 | 23.9 |
| F-2131 | 61-120 | 8.5 | 227.5 | 23.6 | 50.7 | 56.7 | 13.2 | 2.82 | 3.37 | 1.48 | 39.5 |
| BFS-2153 | - | 7.9 | 205.3 | 9.3 | 21.8 | 22.4 | 2.6 | 13.0 | 13.54 | 6.03 | 22.7 |

[a] The sample code represents the sedimentation pond (A-F) and the sample number. Sample BFS-2153 is a fresh BFS from the blast furnace Schwelgern 2 in Duisburg, Germany. All other samples are from the BFS sedimentation pond site in Herne-Wanne, Germany.

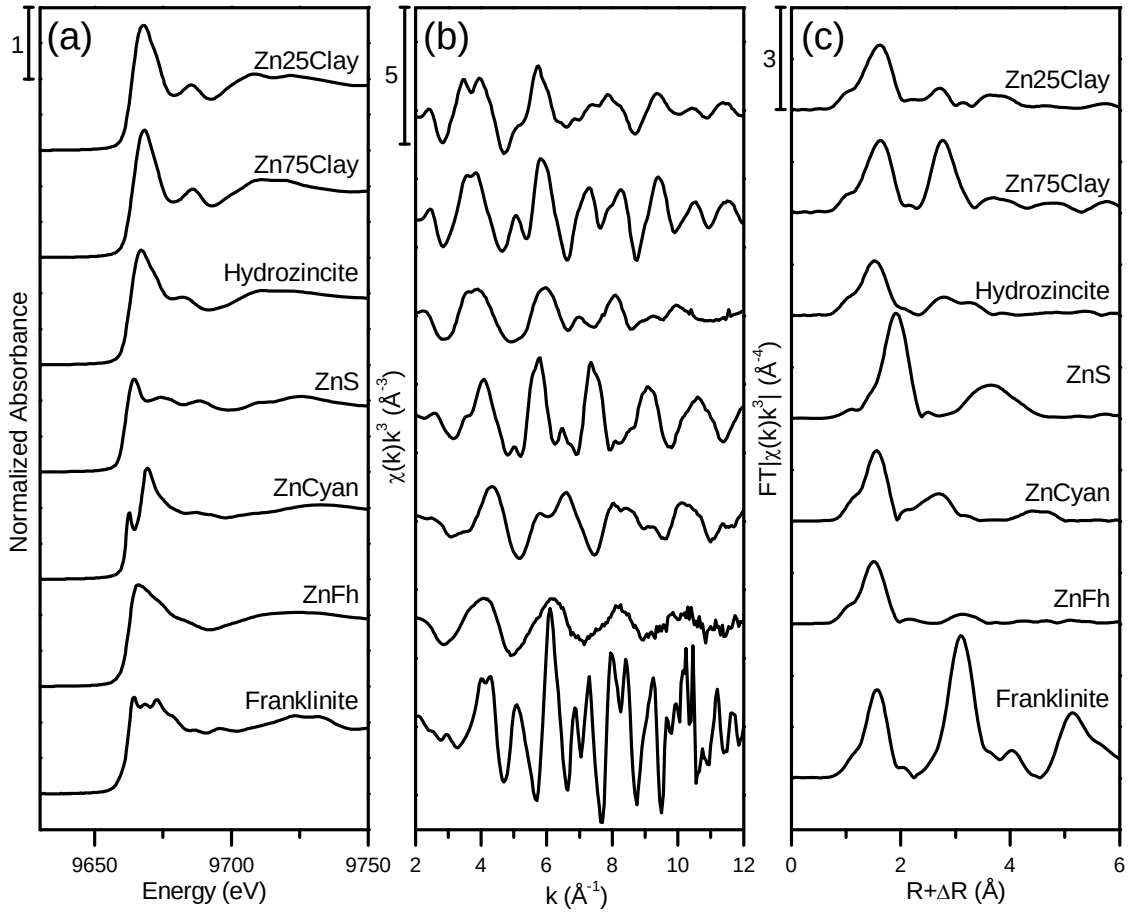


Figure S3. XANES and EXAFS spectra of relevant Zn reference compounds used for linear combination fitting of spectra of BFS samples. Franklinite was never detected in this study, but is shown for comparison because of previous reports that franklinite may occur in BFS. The franklinite spectrum[6] was kindly provided by Andreas Scheinost (ESRF, Rossendorf Beamline).

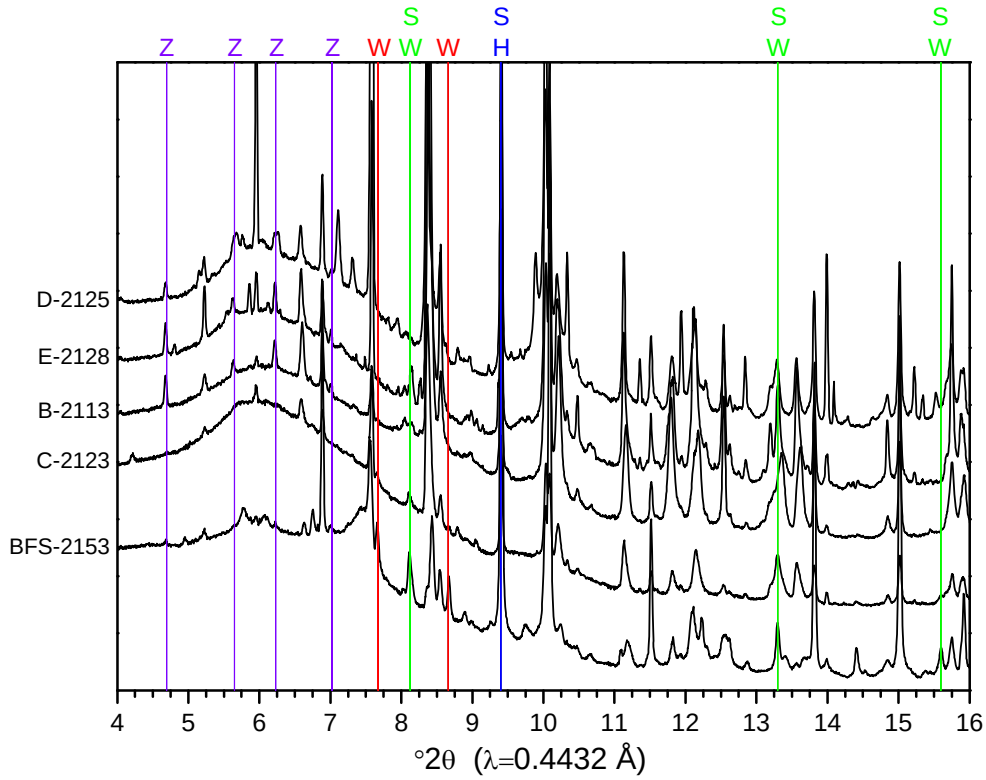


Figure S4. Synchrotron XRD patterns of selected BFS from ponds B to E at Herne-Wanne and one fresh BFS (2153) from the blast furnace Schwelgern 2. The same spectra are shown in Figure 1 over a different °2θ range. Main reflections of Zn phases are marked with colored lines (violet: KZn-cyanoferrate (Z); red: wurtzite (W); green: sphalerite/wurtzite (S/W); blue: sphalerite/hematite (S/H). The incoming X-ray energy was 27.97 keV.

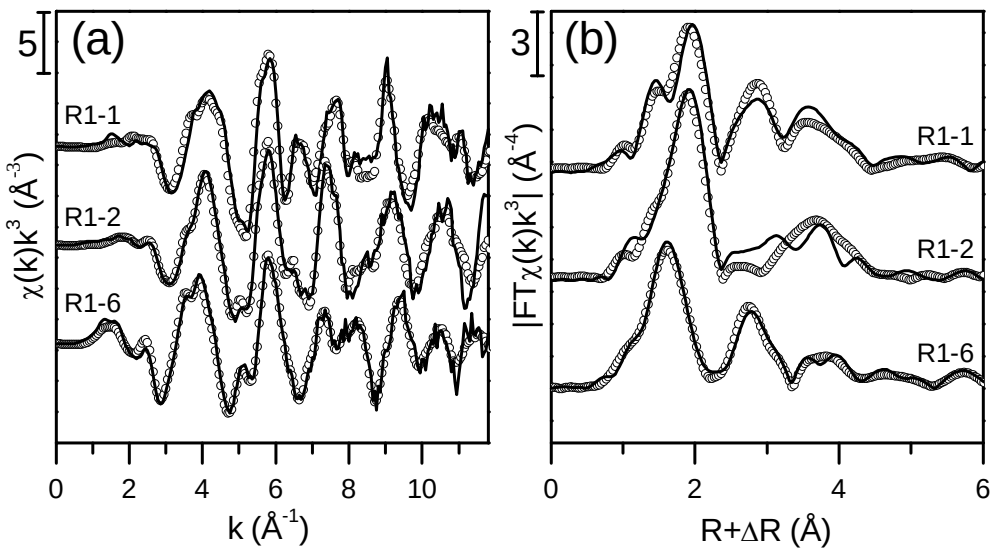


Figure S5. (a) μ-EXAFS chi-functions, and (b) μ-EXAFS Fourier transform magnitude functions of the blast furnace sludge samples (lines) not shown in Figure 3. Symbols represent corresponding linear combination fits (LCF) for EXAFS spectra. LCF fits were done in k-space using a k-range of 3-11 $Å^{-1}$. The fitting results are reported in Table 2.

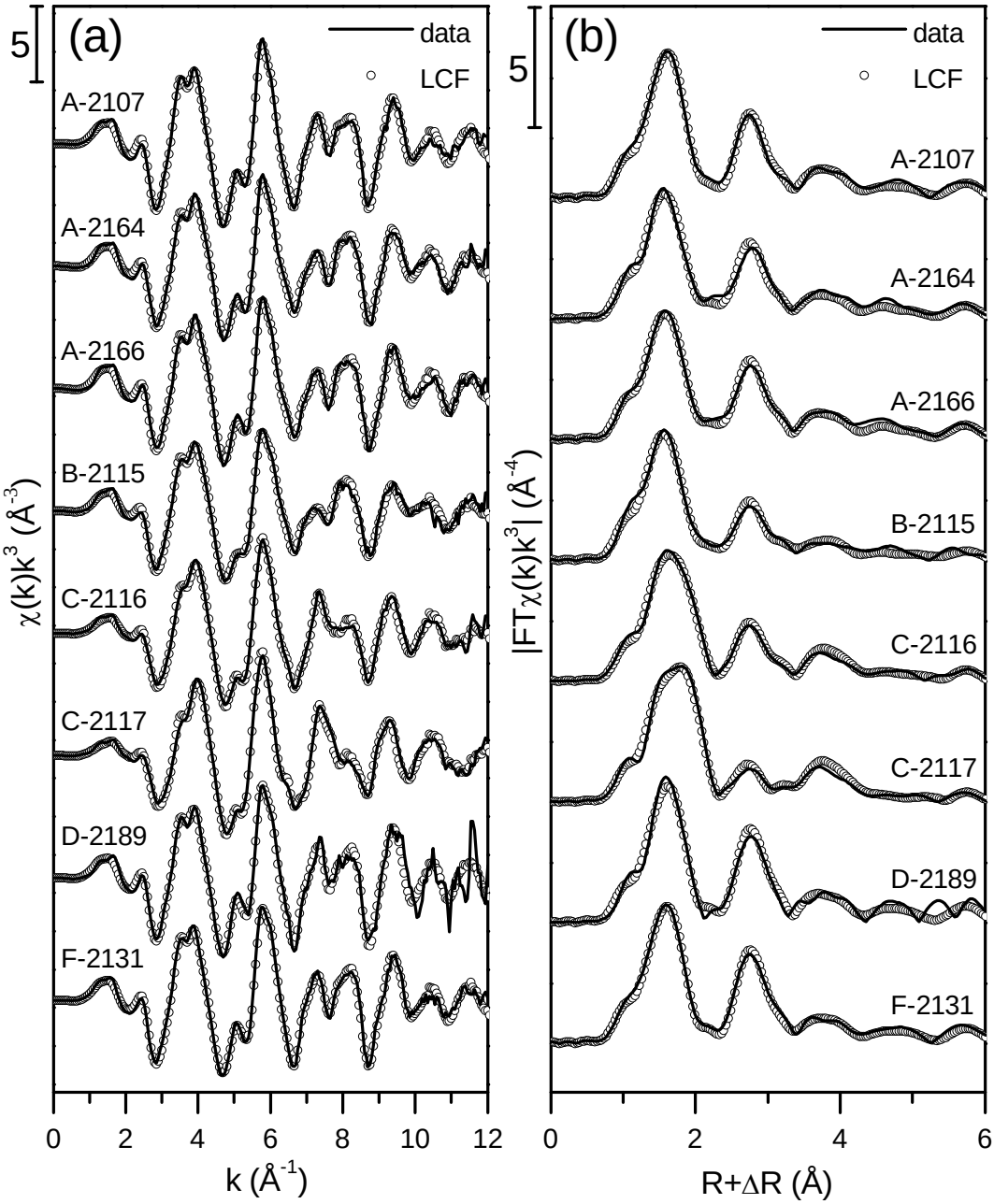


Figure S6. (a) EXAFS chi-functions, and (b) EXAFS Fourier transform magnitude functions of the blast furnace sludge samples (lines) not shown in Figure 4. Symbols represent corresponding linear combination fits (LCF) for EXAFS spectra. LCF fits were done in k-space using a k-range of 3-12 $Å^{-1}$. The fitting results are reported in Table 3.

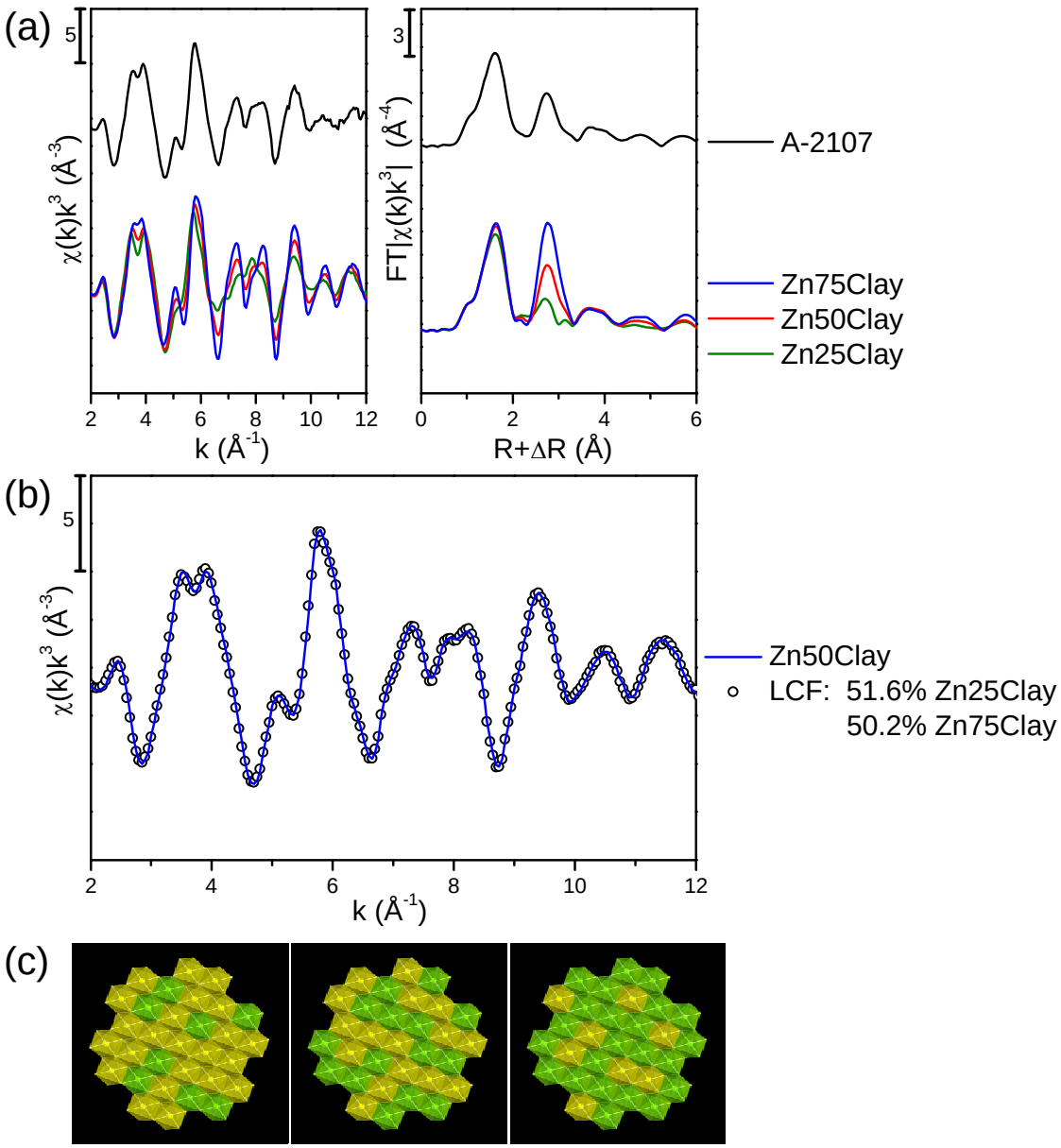


Figure S7. Zn K-edge EXAFS spectra of BFS and synthetic Zn-clays. (a) BFS A-2107 and clays with 75, 50, and 25% Zn in the octahedral sheet. (b) Clay with 50% Zn in the octahedral sheet (Zn50Clay), fitted with a linear combination of 51.6% Zn25Clay and 50.2% Zn75 Clay. (c) Illustration of trioctahedral sheets with 25, 50, and 75% Zn (green) and other lighter elements such as Mg (yellow). Increasing Zn content resulted in an increasing second-shell Zn-Zn backscattering signal in the EXAFS spectra, as observed in panel (a).

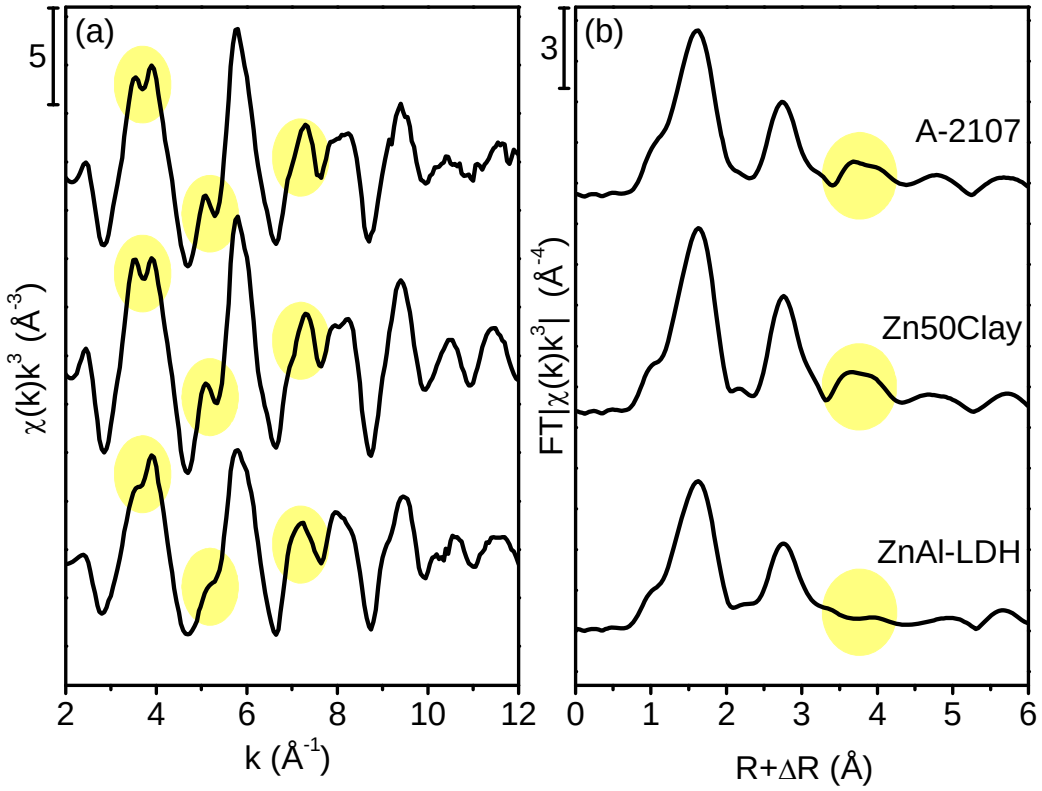


FIGURE S8. Zn K-edge EXAFS spectra of a BFS sample (A-2107), Zn in a clay mineral structure (Zn50Clay), and Zn in layered double hydroxide (ZnAl-LHD). The most prominent differences in the spectra are highlighted in yellow color. The BFS spectrum is more similar to the Zn50clay than to the ZnAl-LDH reference spectrum.

## References


1. Mansfeldt, T.; Dohrmann, R. Chemical and mineralogical characterization of blast-furnace sludge from an abandoned landfill. *Environ. Sci. Technol.* **2004,** *38*, (22), 5977-5984.
2. Schuwirth, N.; Voegelin, A.; Kretzschmar, R.; Hofmann, T. Vertical distribution and speciation of trace metals in weathering flotation residues of a zinc/lead sulfide mine. *J. Environ. Qual.* **2007,** *36*, (1), 61-69.
3. Jacquat, O.; Voegelin, A.; Villard, A.; Marcus, M. A.; Kretzschmar, R. Formation of Zn-rich phyllosilicate, Zn-layered double hydroxide and hydrozincite in contaminated calcareous soils. *Geochim. Cosmochim. Acta* **2008,** *72*, (20), 5037-5054.
4. Voegelin, A.; Pfister, S.; Scheinost, A. C.; Marcus, M. A.; Kretzschmar, R. Changes in zinc speciation in field soil after contamination with zinc oxide. *Environ. Sci. Technol.* **2005,** *39*, (17), 6616-6623.
5. Jacquat, O.; Voegelin, A.; Juillot, F.; Kretzschmar, R. Changes in Zn speciation during soil formation from Zn-rich limestones. *Geochim. Cosmochim. Acta* **2009,** *73*, (19), 5554-5571.
6. Roberts, D. R.; Scheinost, A. C.; Sparks, D. L. Zinc speciation in a smelter-contaminated soil profile using bulk and microspectroscopic techniques. *Environ. Sci. Technol.* **2002,** *36*, (8), 1742-1750.
7. Malinowski, E. R.; McCue, M. Qualitative and quantitative determination of suspected components in mixtures by target transformation factor analysis of their mass spectra. *Anal. Chem.* **1977,** *49*, (2), 284-287.